Scientific Research Publishing

Open Journal of Applied Sciences, 2024, 14, 1237-1250
https://www.scirp.org/journal/ojapps
ISSN Online: 2165-3925
ISSN Print: 2165-3917

# Analysis of Influence on Aerodynamic Noise of Wind Turbine Blades under Different Pitch Angles

**Ruirong He, Houcai Liu, Huimin Kang, Jiale Xi**

School of Mechanical and Electrical Engineering, Hunan University of Science and Technology, Xiangtan, China
Email: qwe578204617@163.com

**How to cite this paper:** He, R.R., Liu, H.C., Kang, H.M. and Xi, J.L. (2024) Analysis of Influence on Aerodynamic Noise of Wind Turbine Blades under Different Pitch Angles. *Open Journal of Applied Sciences*, **14**, 1237-1250.
https://doi.org/10.4236/ojapps.2024.145080

**Received:** April 10, 2024
**Accepted:** May 11, 2024
**Published:** May 14, 2024



## Abstract

Aiming at the influence of blade pitch Angle on aerodynamic noise of wind turbines, the sound field and flow field distribution at 0˚, 5˚, 10˚ and 15˚ are calculated by numerical simulation. Then, through the distribution of pressure field and velocity field calculated by flow field, the influence of different pitch angles on wind turbine blade aerodynamic noise and the reasons for its influence are analyzed. The results show that when the pitch Angle increases within 0˚ - 10˚, the aerodynamic noise pressure level of the blade decreases. However, the sound pressure level of aerodynamic noise increases in the range of 10˚ - 15˚. The changes of static pressure gradient and pressure pulsation on the blade surface make the aerodynamic noise change, and the changes of the two are positively correlated. At the same time, the fluid velocity and fluid motion state on the blade surface are closely related to the aerodynamic noise of the blade. The greater the fluid velocity, the more complex the fluid motion state and the greater the turbulent kinetic energy of the wind turbine blade, and the aerodynamic noise of the wind turbine blade will also increase.

## Keywords

Pitch Angle, Aerodynamic Noise, Static Pressure Gradient, Fluid Motion, Numerical Simulation

## 1. Introduction

In the past decade, people have been developing and utilizing clean energy and renewable energy, such as wind, solar, hydrogen and so on. Among them, the development and utilization of wind energy has made great progress in all countries in the world, and the proportion of wind energy consumption is also in-

creasing, which can fully reflect the development and utilization of wind energy is one of the key development areas today. With the large-scale design and development of wind turbines, the impact of huge wind turbines on people's living environment is also increasing, and the more prominent problem is the noise problem of wind turbines [1] [2].

Researchers at home and abroad have done a lot of research on the factors affecting the aerodynamic noise of wind turbines. Kevin Volkmer [3] *et al.* reduced aerodynamic noise by optimizing blade appearance, applying boundary layer tripping and increasing serrated blade trailing edge. The research shows that different blade types and thickens, tripping and serrated trailing edge can all reduce noise, but always reduce the output power of wind turbines. Weijie Wang [4] *et al.* respectively studied the variation rule of low-frequency noise of wind turbines with rated power ($P_w$) of 1.5 MW and 4.5 MW during operation and shutdown. Compared with 1.5 MW wind turbines, 4.5 MW wind turbines have larger noise sound pressure level in low frequency band, especially in the 80 - 300 Hz frequency band. The noise pressure level within 250 Hz changes obviously with the wind speed. Christof Ocker [5] *et al.* conducted wind tunnel tests on different blade geometry (NACA 4412, Clark-Y and sickle shapes), five depression angles ($\beta$) between −2 and 8˚, and five wind speeds ($v_\infty$) between 5 and 13 m/s. The results showed that the distribution and intensity of sound sources were highly correlated with wind speed and blade geometry. Vinit V. Dighe [6] *et al.* studied the aeroacoustic performance of duct type wind turbine under yaw inflow conditions. The power spectrum analysis shows that the broadband noise contribution of DonQi D5 model is higher under both yaw inflow and non-yaw inflow conditions. The broadband noise is the trailing edge noise of turbulent boundary layer caused by turbulent flow structure on the pipeline surface. Sun Pingling [7] *et al.* conducted simulation and test analysis on aerodynamic noise of a wind turbine in a certain place in Shandong province, and studied the attenuation characteristics of aerodynamic noise and its spectrum characteristics under different wind speeds. The results show that the aerodynamic noise acoustic power level ($APL$) increases with the increase of wind speed, and becomes stable when the rated wind speed is reached. Xing Jianfeng *et al.* [8] studied the influence of aero foil concave variation on wake noise under stable and unsteady inflow conditions, and pointed out that aero foil concave variation blades can effectively reduce noise, and the noise reduction effect under unsteady inflow conditions is better than that under stable inflow conditions. Wu Weimin [9] *et al.* analyzed the influence of different tip structures on flow field and noise field by changing the fold Angle ($\theta$) of blade tip pairs. The results show that the fusion tip structure can affect the generating position and intensity of tip vortices to a certain extent, thus reducing the aerodynamic noise of blades. Li Yixiao [10] *et al.*, by reconstructing the trailing edge of wind power blades, analyzed that the asymmetric saw tooth trailing edge has a good noise reduction effect in the low and medium frequency bands, and pointed out that both the width ($w$) and spacing ($d$) of saw tooth can effectively reduce aerodynamic noise.

Although a lot of research work has been carried out in the aerodynamic noise analysis of wind turbines, most of the research focuses on the analysis of aerodynamic noise and noise reduction effect by changing blade shape, blade trailing edge structure, blade tip shape, etc. However, there are few studies on the effect of blade pitch Angle on aerodynamic noise of wind turbines. The change of blade pitch Angle can make the velocity and pressure of the blade surface change, which leads to the change of aerodynamic noise of the blade. Therefore, this study employs numerical simulation to investigate the impact of varying blade pitch angles on aerodynamic noise generated by wind turbine blades, through analysis of pressure field distribution, velocity field distribution, and aerodynamic noise field distribution on the surface of the blades. This study provides some reference value for the analysis of wind turbine blade aerodynamic noise reduction.

## 2. Numerical Simulation Analysis Method

### 2.1. FW-H acoustic Analogy Equation

Ffowcs Williams and Hawkings based on Lighthill's equation, by introducing the effect of solid boundary, so as to more accurately predict the sound generated by the fluid near the solid surface of the sound analogy equation, known as the FW-H equation. FW-H acoustic analogy equation is as follows [11]:

$$\begin{aligned}&\frac{1}{c_0^2}\frac{\partial^2}{\partial t^2}\left[pH(f)\right]-\nabla^2\left[pH(f)\right]\\&=\frac{\partial}{\partial t}-\left[\rho_0 v_i\frac{\partial f}{\partial x_i}\delta(f)\right]-\frac{\partial}{\partial x_i}\left[p_{ij}\frac{\partial f}{\partial x_i}\delta(f)\right]+\frac{\partial^2}{\partial x_i\partial x_j}\left[T_{ij}H(f)\right]\end{aligned}\tag{1}$$

where $T_{ij}=\rho u_i u_j+p_{ij}-\delta_{ij}c_0^2\rho$, $H(f)$ is Heaviside's generalized function, $\delta(f)$ is a Dirac function, $p_{ij}$ is the stress tensor of the surface, $T_{ij}$ is Lighthill's stress tensor.

The first term on the right of formula (1) is the surface sound source distributed on the surface of the object; the second term is the surface sound source formed by the pressure pulsation caused by the change of static pressure gradient and stress tensor of the surface of the object; the third term is the volume sound source caused by the fluid pulsation outside the surface of the object.

### 2.2. Large Eddy Simulation (LES) Calculation Model

The calculation method of large eddy simulation is to calculate the turbulence model after filtering. Its core processing method is to calculate the large vortex and the small vortex separately in the turbulent flow. The structure of large vortices has a great influence on the flow field and plays a leading role in the turbulent flow field. The small vortices are filtered and solved by additional equations.

The incompressible N-S equation processed by the filter function is as follows [12]:

$$\frac{\partial \rho}{\partial t}+\frac{\partial}{\partial x_i}\left(\rho \bar{u}\right)=0 \tag{2}$$

$$\frac{\partial}{\partial t}\left(\rho \bar{u}\right)+\frac{\partial}{\partial x_j}\left(\rho \bar{u}\cdot \bar{v}\right)=\frac{\partial}{\partial x_j}\left(\mu \frac{\partial \bar{u}}{\partial x_j}\right)-\frac{\partial \bar{p}}{\partial x_i}-\frac{\partial \tau_{ij}}{\partial x_j} \tag{3}$$

where $\bar{u},\bar{v}$ are the filtered velocity components in the direction *i* and *j*, respectively; $\bar{p}$ is the filtered pressure; $\tau_{ij}$ is the stress of the subgrid, it is defined as:

$$\tau_{ij}=\rho\overline{uv}-\rho\bar{u}\cdot\bar{v} \tag{4}$$

The filtered subgrid needs to be processed by SGS model, whose equation is as follows:

$$\tau_{ij}=\frac{1}{3}\tau_{kk}\delta_{ij}-2\mu_t\bar{S}_{ij} \tag{5}$$

where, $\mu_t$ is the subgrid turbulent viscosity coefficient, $\delta_{ij}$ is the stress tensor, and $\bar{S}_{ij}$ is the mesh mixing length.

## 2.3. Influence of Pitch Angle on Aerodynamic Noise

When the wind speed is lower than the rated wind speed, the pitch Angle is generally near $\beta = 0$, so that the wind energy utilization coefficient is stable and maximum to meet the requirements of grid-connected power generation. When the wind speed is higher than the rated wind speed, the speed of the impeller is controlled at the highest speed value, and the wind energy utilization coefficient is changed by changing the size of the pitch Angle, so as to ensure the stability of the output power of the system.

According to literature [13], the fitting function of wind energy utilization coefficient in practical projects is as follows:

$$C_p\left(\lambda,\beta\right)=\left(0.44-0.0167\beta\right)\sin\left[\frac{\pi\left(\lambda-3\right)}{15-0.3\beta}\right]-0.00184\left(\lambda-3\right)\beta \tag{6}$$

where $\lambda$ is the tip ratio. It can be concluded from the above formula that the wind energy utilization coefficient $C_p$ decreases with the increase of pitch Angle $\beta$.

When pitch angle $\beta$ was changed, tangential induction factor and axial induction factor on blade were also changed. When the pitch Angle is known to be $\beta$, the induction factor value can be calculated by iterative method [14]. The iterative calculation flow chart is shown in **Figure 1**. After determining the axial induction factor $a$ and tangential induction factor $a'$, the relative synthesis velocity $v_l$ on the blade element can be calculated by combining the rotational speed Ω of the impeller and the inlet wind speed $v_\infty$ [14]:

$$v_l=\sqrt{v_\infty^2\left(1-a\right)^2+\Omega^2l^2\left(1+a'\right)^2} \tag{7}$$

According to Powell's vortex sound theory equation [15]:

$$\frac{1}{c_0^2}\frac{\partial^2 p}{\partial t^2}-\nabla^2 p=\nabla\cdot\left[\rho_0\left(\vec{\omega}\times\vec{v}_l\right)+\rho_0\nabla\frac{\vec{v}_l^{\,2}}{2}\right] \tag{8}$$

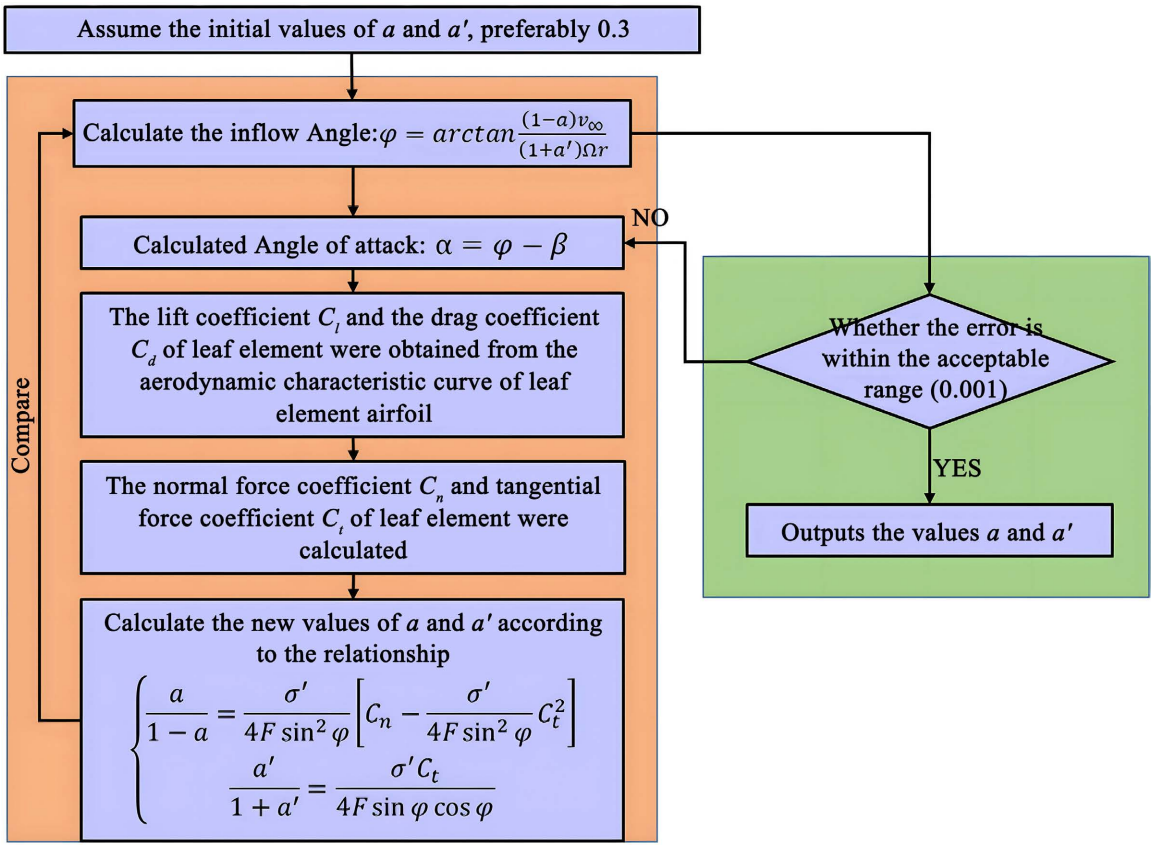


**Figure 1.** Induction factor iterative calculation flow chart.

where, $\nabla$ is the Hamiltonian operator, $\rho$ is the fluid density, $t$ is the time, $p$ is the fluid pressure, and $\vec{\omega}$ is the vorticity. The left differential of the equation is the wave equation of sound pressure, which represents the acoustic characteristics of sound pressure propagation. On the right side of the equation is the sound source term, which represents the sound source of the sound wave radiation.

From the above equation, it can be seen that when blade pitch Angle $\beta$ changes, axial induction factor and tangential induction factor change, and the relative synthesis speed of leaf elements also changes, which leads to the change of sound pressure.

## 3. Numerical Model

### 3.1. Numerical Geometry Model

Taking XE122-2500 2.5 MW wind turbine blades as the research object, the blade model is shown in Figure 2. The blade length is 59.5 m, the rotating diameter of the impeller is 122 m, the rated power is 2.5 MW, the rated speed is 11.5 r/min, the maximum speed is 12.8 r/min, and the sweep area of the wind wheel is 11741.5 $m^2$.

In order to improve the convergence of numerical simulation calculation, this paper simplifies the model of wind turbine, ignoring the hub and tower, that is,

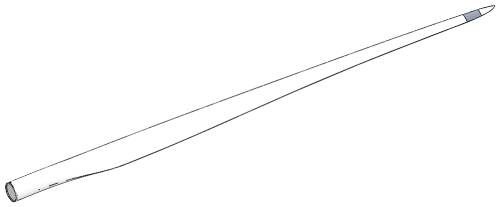

**Figure 2.** 3D model of wind turbine blade.

the model is an impeller formed by three identical blades. On the basis of forming the impeller, the pitch Angle of the impeller model is set to 0˚, 5˚, 10˚ and 15˚ respectively, as shown in **Figure 3**.

The model of the numerical simulation calculation area is designed in the form of a cuboid wind tunnel, as shown in **Figure 4**. The calculation region is divided into two parts: the near-field rotation region near the blade and the outer flow field region. The calculation area of the outer laminar flow field is designed as a cuboid with a length of 8R along the X-axis and a square with a cross-section of 4R × 4R. The axial distance between the center of the impeller and the entrance section is 3R, and the axial distance between the impeller and the exit section is 5R. The rotation area of the near flow field is designed as a cylinder with a radius of 1.25R and an axial length of 0.5R. The distance between the front section and the center of the impeller is 0.2R, and the distance between the back section and the center of the impeller is 0.3R.

### 3.2. Mesh Generation

The mesh division of the numerical simulation area is segmented, including the volume grid of the outer laminar flow field, the volume grid of the near flow field rotation area and the surface grid of the blade surface. The model features of the outer fluid field region are relatively simple and the outline is relatively large. The hexahedral mesh is sufficient to reflect the features of the outer fluid field. However, the characteristics of the near-flow field rotation region are relatively complex, between the outer fluid field region and the blade, and the outline is relatively sharp, requiring the use of unstructured tetrahedral mesh. Regular quadrilateral surface mesh is used on the blade surface to generate boundary layer mesh. The growth rate of the boundary layer is set to 1.15, the thickness of the first layer mesh of the boundary layer is calculated according to the $y+$ value [16], and the number of layers of the boundary layer is set to 20.

In order to strike a balance between calculation accuracy and calculation efficiency, three groups of grids were set up to calculate the lift coefficient to verify the quantitative independence of the meshes. The lift coefficients calculated by each grid group are shown in **Table 1**. The $y+$ value of the first mesh is 7, and the number of generated meshes is 5.42 million. The $y+$ value of the second mesh is 5, and the number of generated meshes is 8.25 million. The third set of meshes has a $y+$ value of 3, and the number of generated meshes is 10.67 million. After calculation, the relative error of lift coefficient of each group is less than

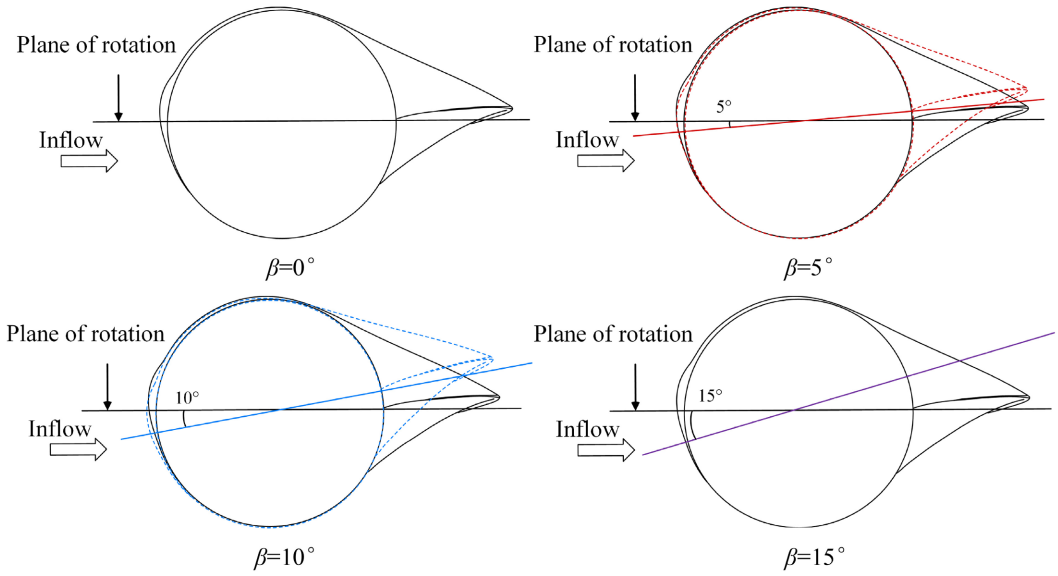


**Figure 3.** Model of blade pitch Angle at four different angles.

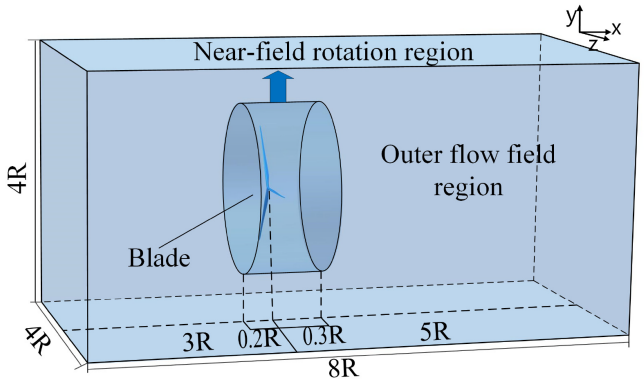


**Figure 4.** Numerical simulation to calculate the three-dimensional model of the region.

**Table 1.** Mesh number independence verification.

| Number | Mesh quantity | Lift coefficient |
|---|---|---|
| 1 | $5.42 \times 10^6$ | 0.213 |
| 2 | $8.25 \times 10^6$ | 0.210 |
| 3 | $1.06 \times 10^7$ | 0.211 |

2%, and the error is relatively small. Therefore, in order to save calculation time, this paper uses a mesh number of 5.42 million for numerical simulation.

### 3.3. Setting of Boundary Conditions

Numerical simulation was performed using ANSYS Fluent finite element software. k-epsilon model was used for steady state turbulence model, and large eddy simulation (LES) turbulence model was used for transient calculation. The inlet boundary is set as the velocity inlet, and the flow rate is 12 m/s; The outlet boundary is set as the pressure outlet, and the pressure value is the standard at-

mospheric pressure; The blade boundary is set to the wall surface, and the speed is set to 11.5 r/min, regardless of blade deformation. The rotation area of the near flow field rotates simultaneously with the blade, and the rotation mode adopts the motion reference frame MRF. The center of the impeller is the rotation center, and the rotation direction is the positive direction of the X-axis. The calculated residual is set to $1 \times 10^{-6}$.

## 4. Analysis of Numerical Results

### 4.1. Sound Source Distribution of Aerodynamic Noise at Different Pitch Angles

Figure 5 shows the distribution cloud view of sound pressure level of pneumatic

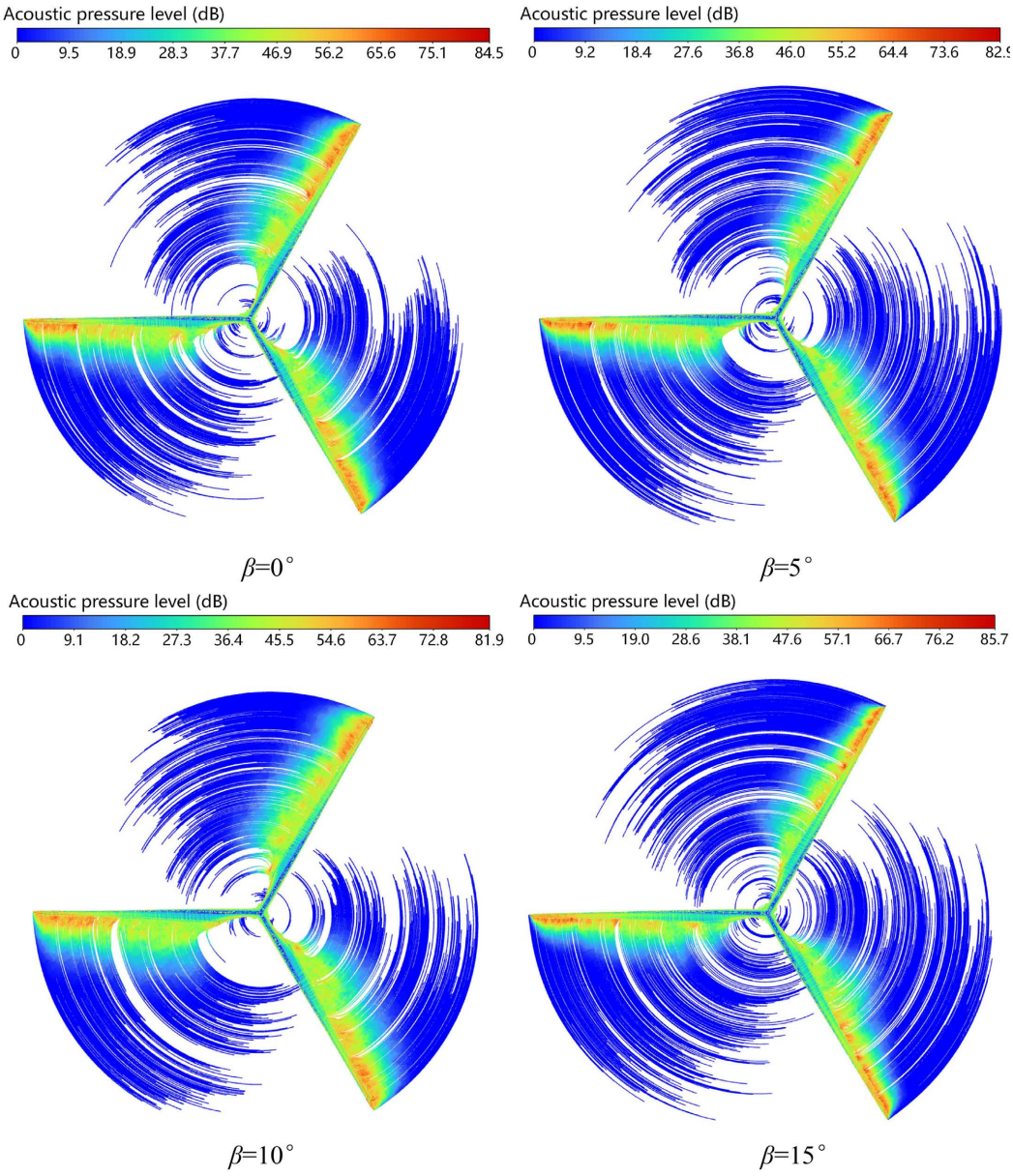


Figure 5. Cloud view of sound pressure level distribution of pneumatic noise under different pitch angles.

noise of wind turbine under different pitch angles obtained by numerical simulation. It can be seen from the figure that the maximum sound pressure level of blade aerodynamic noise under four different pitch angles is distributed on about 65% - 95% blade span segments, indicating that the sound sources of wind turbine blade aerodynamic noise under different pitch angles are mainly distributed on 65% - 95% blade span segments. At the same time, it can be concluded from the maximum sound pressure level of aerodynamic noise that when the blade pitch Angle increases within 0˚ - 10˚, the aerodynamic noise sound pressure level decreases with the increase of the pitch Angle. For example, the maximum noise pressure level value when the pitch Angle is 0˚ is 84.5 dB, the maximum noise pressure level value when the pitch Angle is 5˚ is 82.9 dB, and the maximum noise pressure level value when the pitch Angle is 10˚ is 81.9 dB. However, when the blade pitch Angle increases within 10˚ - 15˚, the sound pressure level of aerodynamic noise increases with the increase of the pitch Angle. That is, when the pitch Angle is 15˚, the maximum noise pressure level value is 85.7 dB.

### 4.2. Pressure Field Distribution at Different Pitch Angles

Figure 6 shows the cloud view of static pressure distribution on the blade surface

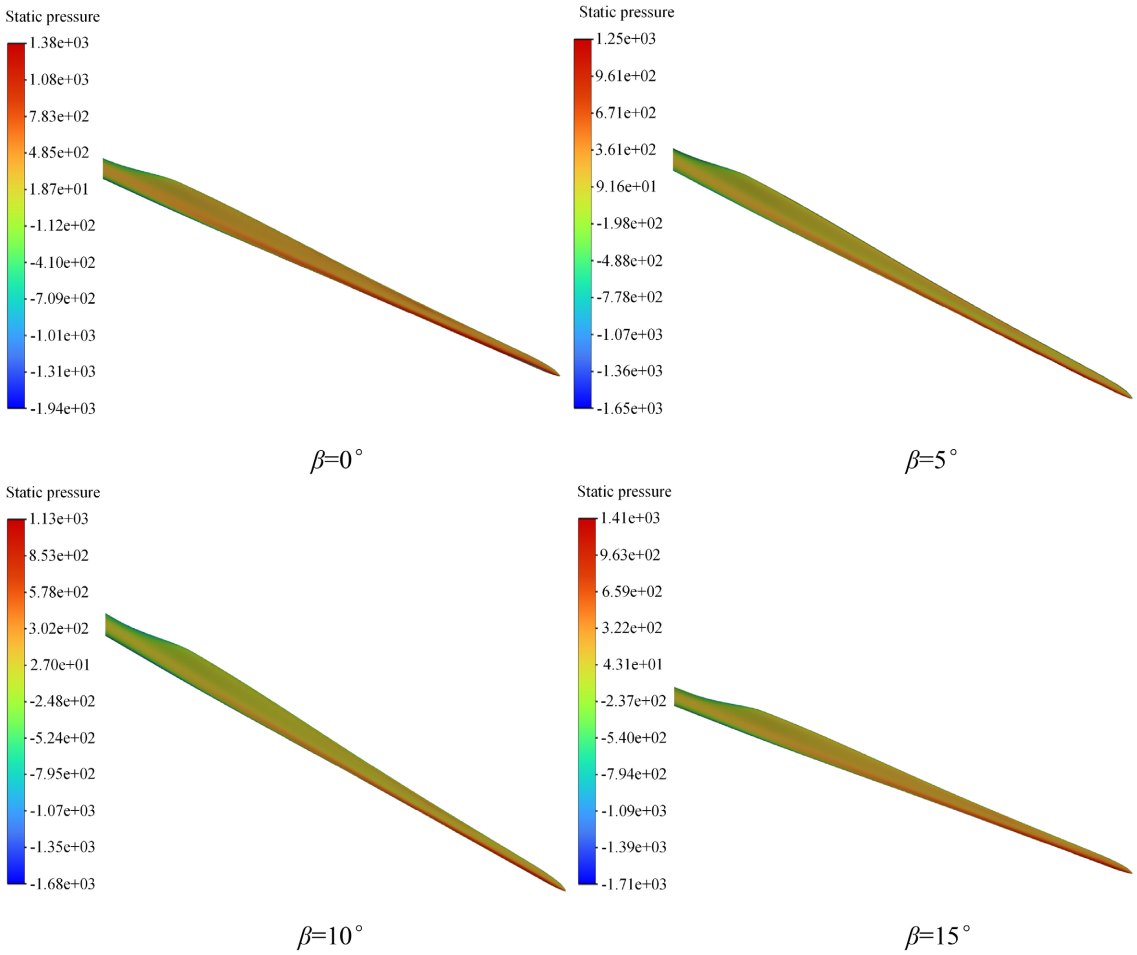


Figure 6. Static pressure distribution cloud image at different pitch angles (pa).

at different pitch angles. It can be seen from the cloud view that the maximum static pressure on the blade surface is mainly distributed near the tip of the blade, about 65% - 95% of the blade span. When the blade pitch Angle changes in the range of 0˚ - 10˚, the static pressure on the blade surface decreases with the increase of the pitch Angle, and the static pressure gradient and pressure pulsation also decrease with the increase of the pitch Angle; When the blade pitch Angle increases from 10˚ to 15˚, the static pressure on the blade surface increases, and the static pressure gradient and pressure pulsation also increase. For example, when the blade pitch Angle is 0˚, the static pressure gradient is $3.32 \times 10^3$ pa. When the blade pitch Angle is 5˚, the static pressure gradient is $2.9 \times 10^3$ pa. When the blade pitch Angle is 10˚, the static pressure gradient is $2.81 \times 10^3$ pa. The blade pitch Angle is 15˚ and the static pressure gradient is $3.39 \times 10^3$ pa.

According to formula (1), static pressure gradient and pressure fluctuation are the main factors affecting aerodynamic noise. According to the analysis of Figure 5 and Figure 6, when the blade pitch Angle is less than 10˚, the static pressure gradient and pressure pulsation on the blade surface decrease with the increase of the blade pitch Angle, and the aerodynamic noise pressure level of the blade also decreases; When the blade pitch Angle is greater than 10˚, the static pressure gradient and pressure pulsation of the blade surface increase with the increase of the blade pitch Angle, and the aerodynamic noise pressure level of the blade also increases.

### 4.3. Velocity Field Distribution at Different Pitch Angles

Figure 7 is the vector diagram of blade surface velocity distribution under different pitch angles. As can be seen from the figure, the closer to the tip of the blade, the greater the fluid velocity on the blade surface, and the denser the arrows on the vector diagram, which are distributed on 65% - 95% of the blade span segments. When the pitch Angle increases in the range of 0˚ - 10˚, the fluid velocity near the blade tip gradually decreases, and the arrows on the velocity vector diagram are gradually sparse, the state of fluid motion also become eases gradually. However, when the pitch Angle increases in the range of 10˚ - 15˚, the fluid speed suddenly increases, the arrows on the velocity vector diagram become denser, and the fluid motion state becomes intense, which is due to the stalling separation flow phenomenon on the blade surface, making the flow state complicated.

The fluid movement was further analyzed, and four monitoring cross sections were selected on the 65% - 95% span of the blade, which were located at the positions of 65%, 75%, 85% and 95% of the blade span, respectively. The distribution of turbulent kinetic energy on each monitoring section was shown in Figure 8. It can be seen from the figure that when the pitch Angle increases in the range of 0˚ - 10˚, the size of turbulent kinetic energy on each span section decreases with the increase of pitch Angle, and the distribution range of turbulent kinetic

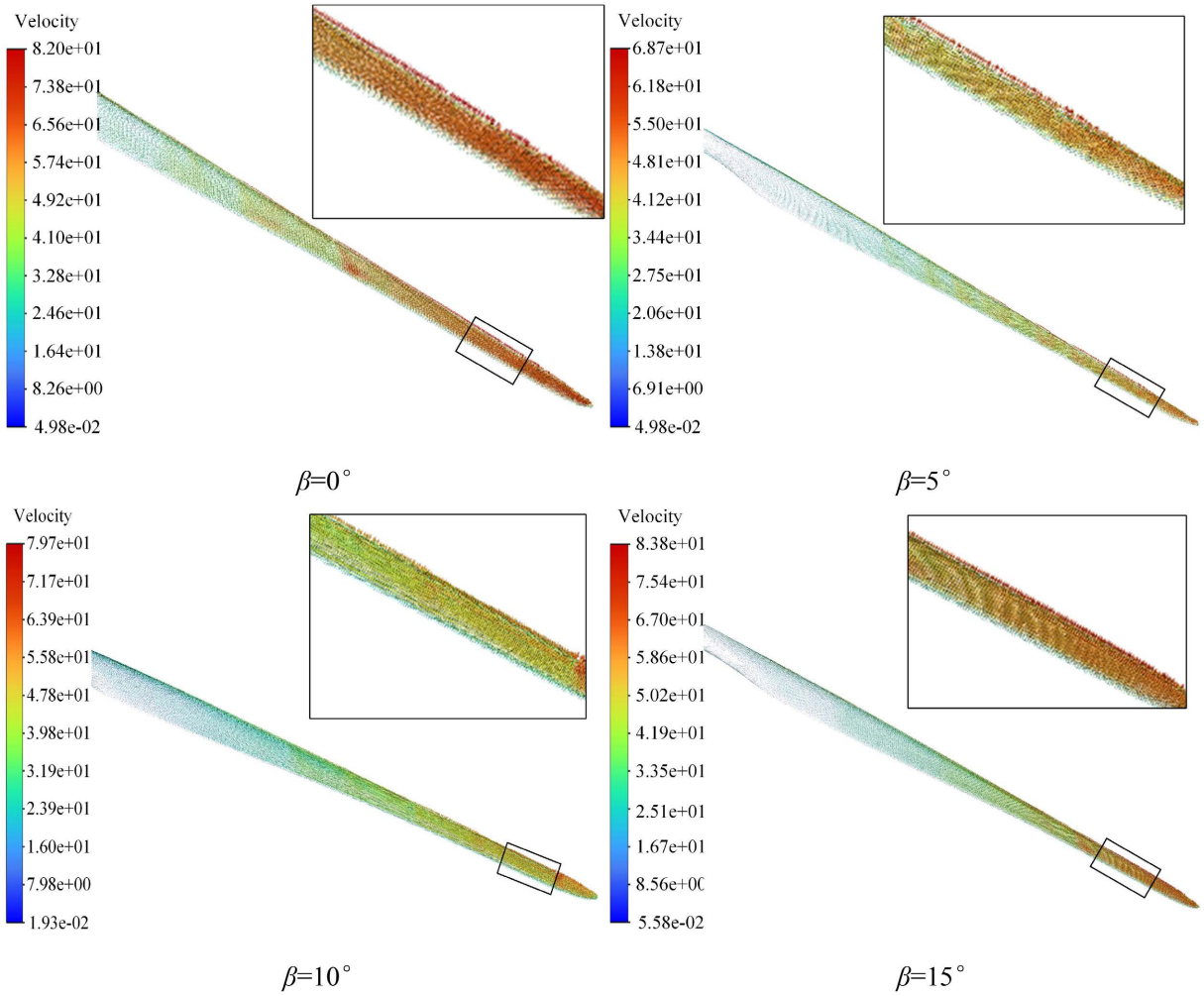


**Figure 7.** Vector diagram of blade surface velocity distribution under different pitch angles (m/s).

energy increases with the increase of pitch Angle. When the pitch Angle increases in the range of 10˚ - 15˚, although the distribution range of turbulent kinetic energy on each span section also increases with the increase of pitch Angle, the turbulent kinetic energy is significantly larger than that in the range of 0˚ - 10˚.

According to fluid mechanics [17], when the turbulent kinetic energy on each cross-section increases within the range of 0˚ - 10˚ pitch Angle, due to the dissipative effect of vortices in turbulence, the large vortices are split into multiple small vortices, which reduces the intensity of vortices and expands the distribution range of vortices, thus leading to a decrease in the sound pressure level of the wind turbine aerodynamic noise sound source. However, when the pitch Angle increases within the range of 10˚ to 15˚, even if there is the dissipation effect of vortices in turbulence, the stalling separation phenomenon makes the fluid motion complicated, the turbulent kinetic energy becomes larger, and the intensity of vortices becomes larger, so that the sound pressure level of the wind turbine aerodynamic noise source also increases.

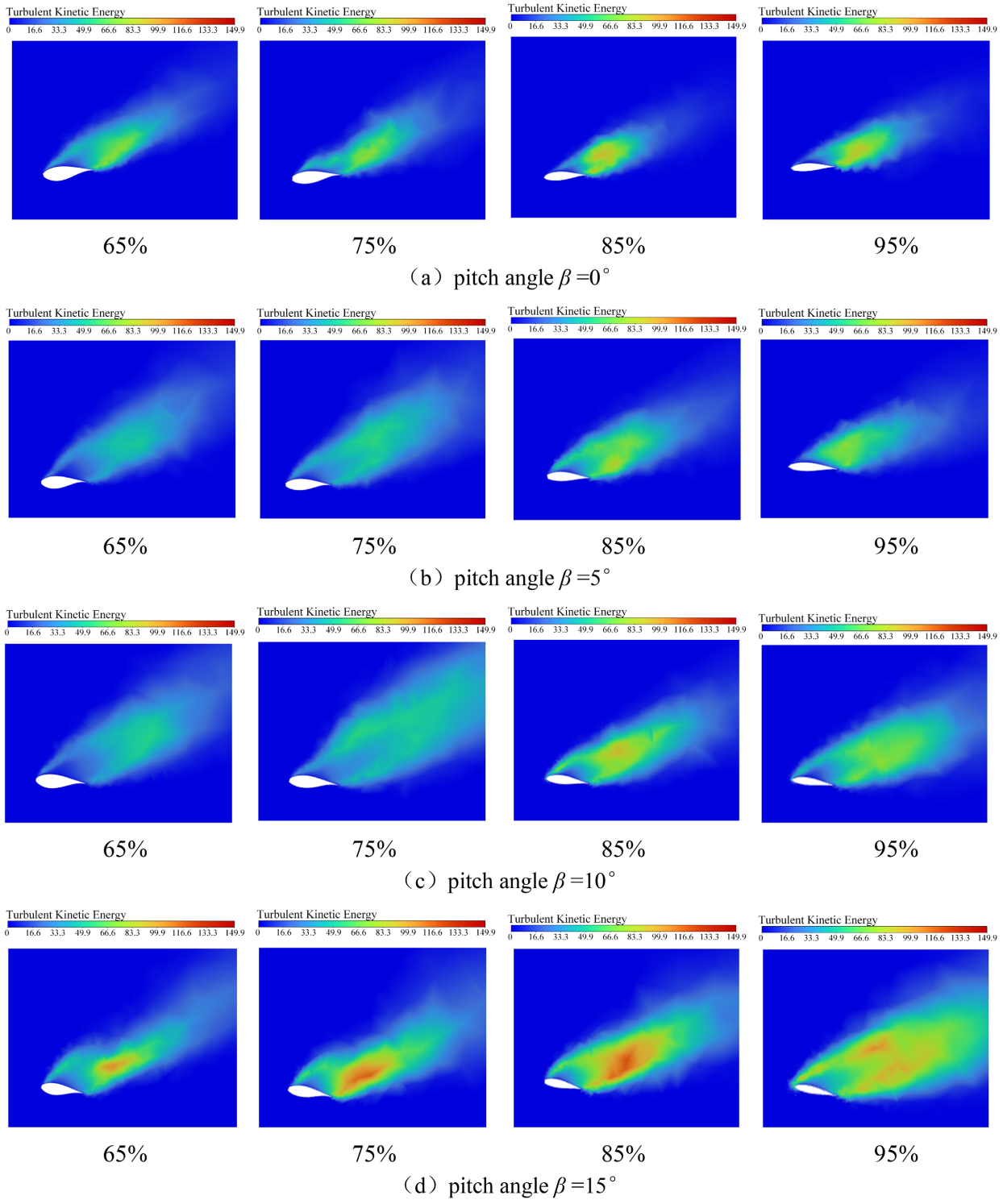


**Figure 8.** Turbulent kinetic energy distribution of each monitoring section at different pitch angles (kg·m²/s²).

## 5. Conclusions

In this paper, the finite element simulation software ANSYS Fluent was used to numerically simulate wind turbine blade aerodynamic noise under different blade pitch angles. By analyzing blade surface pressure distribution and blade

surface velocity distribution, the influence of different blade pitch angles on blade aerodynamic noise was studied. The conclusions are as follows:

1) The aerodynamic noise of the blade is mainly distributed in 65% - 95% of the blade span segments, and the maximum sound pressure level of the aerodynamic noise decreases when the pitch Angle increases in the range of 0˚ - 10˚. However, when the pitch Angle increases in the range of 10˚ - 15˚, the maximum sound pressure level of aerodynamic noise increases.

2) Through the static pressure analysis of the blade surface, the static pressure gradient and pressure pulsation of the blade surface decrease, and the aerodynamic noise of the blade decreases accordingly; The aerodynamic noise of the blade increases with the increase of static pressure gradient and pressure pulsation on the blade surface.

3) The motion state of the fluid on the blade surface becomes moderate when the pitch Angle is 0˚ - 10˚, and the fluid movement becomes complicated when the pitch Angle is 10˚ - 15˚, which is due to the stall separation phenomenon on the blade surface. However, the stalling separation phenomenon increases the turbulent kinetic energy and vortex intensity, which leads to the increase of aerodynamic noise pressure level.

## Acknowledgements

The above study was supported by the National Natural Science Foundation of China (51875198), Key project of Hunan Provincial Department of Education: Research on the Formation and Evolution Mechanism of Oil Film Holes in hydrostatic motorized spindle and its Active Control Method (23A0360) and the Xiangtan Science and Technology Bureau Science and Technology Research Project "Research on Active Control and Evaluation Technology of Variable Mass Unbalanced rotor System of Ultra-High Speed Maglev Permanent Magnet Synchronous motorized spindle" (GX-YB20221004).

## Conflicts of Interest

The authors declare no conflicts of interest regarding the publication of this paper.

## References

[1] Cao, G. (2023) Discussion on the Status Quo and Development Trend of Wind Power Technology. *Scientific and Technological Innovation and Productivity*, **44**, 86-88-91.

[2] Yang, L.N. (2017) Global Wind Power Market Outlook 2017. *Wind Energy*, **3**, 42-43.

[3] Volkmer, K., Kaufmann, N. and Carolus, T.H. (2021) Mitigation of the Aerodynamic Noise of Small Axial Wind Turbines-Methods and Experimental Validation. *Journal of Sound and Vibration*, **500**, Article ID: 116027. https://doi.org/10.1016/j.jsv.2021.116027

[4] Wang, W., Yan, Y., Zhao, Y., *et al.* (2024) Studies on the Experimental Measure-

ment of the Low-Frequency Aerodynamic Noise of Large Wind Turbines. *Energies*, **17**, 1609. https://doi.org/10.3390/en17071609

[5] Ocker, C., Blumendeller, E., Berlinger, P., *et al.* (2022) Localization of Wind Turbine Noise Using a Microphone Array in Wind Tunnel Measurements. *Wind Energy*, **25**, 149-167. https://doi.org/10.1002/we.2665

[6] Dighe, V.V., Avallone, F. and van Bussel, G. (2020) Effects of Yawed Inflow on the Aerodynamic and Aeroacoustic Performance of Ducted Wind Turbines. *Journal of Wind Engineering and Industrial Aerodynamics*, **201**, Article ID: 104174. https://doi.org/10.1016/j.jweia.2020.104174

[7] Sun, P.L., Li, X.P. and Zhao, H.Y. (2022) Noise Characteristics of Wind Turbines. *Environmental Monitoring in China*, **38**, 129-135.

[8] Xing, J.F., Ma, J.L. and Su, H.J. (2023) Study on the Influence of Airfoil Concave Variation on Wind Turbine Aerodynamic Noise under Gust Inflow. *Acta Energiae Solaris Sinica*, **44**, 156-162.

[9] Wu, W.M., Yao, J.Y. and Dai, Y.J. (2020) Research on the Effect of Fusion Tip Structure Changes on the Flow Field and Noise Field in the Tip Region of Wind Turbines. *Acta Energiae Solaris Sinica,* **41**, 190-198.

[10] Li, Y.X., Chen, K. and Gao, R.B. (2022) Effects of Asymmetric Saw Tooth Structure on Aerodynamic Acoustic Performance of Blades. *Acta Energiae Solaris Sinica*, **43**, 336-343.

[11] Farassat, F. and Brentner, K.S. (1998) The Acoustic Analogy and the Prediction of the Noise of Rotating Blades. *Theoretical and Computational Fluid Dynamics*, **10**, 155-170. https://doi.org/10.1007/s001620050056

[12] Song, B.Y. (2023) Research on Aerodynamic Noise Characteristics and Noise Reduction Methods of Wind Turbine Blades. Shanghai University of Electric Power, Shanghai.

[13] Yang, J.S. (2017) Research on Aerodynamic Load Control Strategy of Large Wind Turbine. Shenyang University of Technology, Shenyang. https://doi.org/10.1088/1755-1315/100/1/012175

[14] Yao, X.J. (2012) Wind Turbine Theory and Design. China Machine Press, Beijing, 56-79.

[15] Powell, A. (1964) Theory of Vortex Sound. *Journal of the Acoustical Society of America*, **36**, 177-195. https://doi.org/10.1121/1.1918931

[16] Králik, J. (2016) CFD Simulation of Air Flow over an Object with Gable Roof, Revised with Y+ Approach. *Sbornik Vedeckych Praci Vysoke Skoly Banske - Technicke Univerzity Ostrava. Rada Stavebni*, **16**, 85-94. https://doi.org/10.1515/tvsb-2016-0018

[17] Wang, X.Z. (2018) Physical Fluid Mechanics. Tsinghua University Press, Beijing, 94-116.